Journal of Electronic Materials
https://doi.org/10.1007/s11664-022-10079-x

ORIGINAL RESEARCH ARTICLE

CNT-Supported Multi-Metallic (Ga@PdAgCo) Anode Catalysts: Synthesis, Characterization, and Glucose Electrooxidation Application

Sefika Kaya[1] · **Aykut Caglar**[1,2] · **Hilal Kivrak**[1,3,4]

Received: 15 July 2022 / Accepted: 7 November 2022

Abstract

Here, Ga@PdAgCo catalysts were prepared by sequential reduction using carbon nanotubes (CNT) as support material. The catalysts at different weight percentages were characterized by inductively coupled plasma-mass spectrometry (ICP-MS), transmission electron microscopy (TEM), x-ray photoelectron spectroscopy (XPS), and x-ray diffraction (XRD) analytical techniques. Chronoamperometry (CA), cyclic voltammetry (CV), and electrochemical impedance spectroscopy (EIS) measurements were applied to examine the glucose electrooxidation performance of the catalysts. Among the catalysts, the 7% Ga@PdAgCo(CNT) multi-metallic catalyst provided the best mass activity and specific activity of 231.08 mA/mg Pd and 2.475 mA/cm^2, respectively. EIS results revealed that the 7% Ga@PdAgCo(CNT) catalyst has a faster electron transfer rate with low (632 Ω) charge transfer resistance (Rct). Consequently, the 7% Ga@PdAgCo(CNT) catalyst stands out as a potential anode catalyst for direct glucose fuel cells.

Keywords Ag · Co · Ga · glucose · Pd · carbon nanotube

Introduction

The rapid growth in the global economy and population has created problems such as rapid depletion of existing energy resources, increasing energy demand, and environmental pollution.[1–3] Fuel cells with high efficiency, easy operation, environmentally friendly nature, and renewable energy source are promising compared to other technologies.[4–7] In recent years, liquid fuel cells have gained importance due to the disadvantages of hydrogen production and storage.[8,9] Glucose, which stands out as a liquid fuel, is a simple sugar that is abundant in nature. Glucose is preferred in fuel cell and sensor studies because of its various advantages: it is environmentally friendly, obtainable from agricultural products, non-toxic and non-volatile, and safe to store.[10–12] In direct glucose fuel cells (DGFCs), 24 electrons are theoretically produced with the complete oxidation of glucose to carbon dioxide and provide 2.87×10^6 J/mol of energy (Eqs. 1–3).[13–16]

$$\text{Anode}: \ C_6H_{12}O_6 + 36OH^- \rightarrow 6CO_3^{2-} + 24H_2O + 24e^- \quad (1)$$

$$\text{Cathode}: \ 6O_2 + 24e^- + 12H_2O \rightarrow 24OH^- \quad (2)$$

$$\text{Overall}: \ C_6H_{12}O_6 + 6O_2 + 12OH^- \rightarrow 6CO_3^{2-} + 12H_2O \quad (3)$$

The oxidation reactions, in which 24 electrons are produced, are unlikely to occur. There is mainly partial oxidation of glucose, which involves breaking the C-H bond. In this way, glucose is oxidized to gluconic acid and produces two electrons (Eqs. 4–6).[17–19]

$$\text{Anode}: \ C_6H_{12}O_6 + 2OH^- \rightarrow C_6H_{12}O_7 + H_2O + 2e^- \quad (4)$$

✉ Sefika Kaya
sefikakaya48@gmail.com; sefikakaya@ogu.edu.tr

Hilal Kivrak
hilalkivrak@gmail.com; hilaldemir.kivrak@ogu.edu.tr

1 Department of Chemical Engineering, Faculty of Engineering and Architectural Sciences, Eskisehir Osmangazi University, 26040 Eskisehir, Turkey

2 Department of Chemical Engineering, Faculty of Engineering, Van Yüzüncü Yil University, 65000 Van, Turkey

3 Translational Medicine Research and Clinical Center, Eskisehir Osmangazi University, 26040 Eskisehir, Turkey

4 Department of Chemical Engineering, Faculty of Engineering, Kyrgyz-Turk Manas University, Bishkek, Kyrgyzstan

Published online: 29 November 2022

$$\text{Cathode}: \ 1/2O_2 + 2e^- + H_2O \rightarrow 2OH^- \quad (5)$$

$$\text{Overall}: \ C_6H_{12}O_6 + 1/2O_2 \rightarrow C_6H_{12}O_7 \quad (6)$$

The electrochemical properties and stability of monometallic catalysts can be improved in their bimetallic or trimetallic form by synthesis with noble metals such as Pt, Pd, Au, Ag, Co, Ni, and Fe.[20–22] When metals with different properties are hybridized, they have better electrocatalytic activity than their simple forms owing to the synergistic effect between them.[23–26] Gu et al. investigated the glucose electrooxidation performance of the Ni/Cr/Co catalyst synthesized by thermal decomposition. They observed that the trimetallic catalysts had superior properties including long-term stability, anti-poisoning ability, and reproducibility.[27] Basu et al. studied glucose electrooxidation with carbon-supported bimetallic (PdPt/C) and trimetallic (PdPtAu/C) catalysts. The PtPdAu/C anode catalyst exhibited higher electrocatalytic activity and better stability. They emphasized that the poisoning effect of Pt was reduced by synthesis with Pd and Au.[28] Pd/C, Pd_3Cu/C, and Pd_3Cu-B/C catalysts were improved by Chai et al. for glucose electrooxidation. The better electrocatalytic activity of the Pd_3Cu-B/C catalyst than the others was explained by the synergistic effect between Pd, Cu, and B.[29] Glucose electrooxidation properties of various catalysts in similar studies are presented in Table I.

In the present study, Pd/CNT, PdAgCo/CNT, and Ga@PdAgCo/CNT catalysts at different weight percentages were prepared by $NaBH_4$ reduction and used for glucose electrooxidation. Inductively coupled plasma–mass spectrometry (ICP-MS), transmission electron microscopy (TEM), x-ray photoelectron spectroscopy (XPS), and x-ray diffraction (XRD) analytical techniques were performed for the characterization of the synthesized catalysts. The resistance, stability, and activity of catalysts were determined by electrochemical impedance spectroscopy (EIS), chronoamperometry (CA), and cyclic voltammetry (CV) measurements.

Experimental Studies

Synthesis and Characterization

Pd/CNT and PdAgCo(80:10:10)/CNT catalysts with 10% wt. metal present on carbon nanotubes were synthesized via $NaBH_4$ co-reduction. In the catalyst preparation stage, firstly, precursor metal salts were dissolved in pure water and carbon nanotubes were added. This mixture was stirred for 2 h in an ultrasonic bath. Then, $NaBH_4$ was added dropwise for reduction and stirred for an additional hour. After washing the mixture, it was filtered and dried at 85°C. Ga@PdAgCo(80:10:10)/CNT catalysts at different weight percentages were synthesized via $NaBH_4$ sequential reduction. Determined amounts of $GaCl_3$ salt were weighed and dissolved in pure water. The synthesized PdAgCo(80:10:10)/CNT catalyst was added to this solution. The above-described experimental processes were applied.

ICP-MS, TEM, XPS, and XRD were applied for characterization of the catalysts. XRD (Malvern Panalytical

Table I The glucose electrooxidation properties of various catalysts used in the literature

Catalyst	Reference electrode	Solution	Current density, mA/cm^2	Reference
N-doped few-layer G/ITO	Ag/AgCl	1 M KOH + 0.5 M $C_6H_{12}O_6$	9.12	30
ITO G7/ITO	Ag/AgCl	1 M KOH + 0.5 M $C_6H_{12}O_6$	1.56 6.58	31
Pt-G/ITO Au-G/ITO G/ITO ITO	Ag/AgCl	1 M KOH + 0.5 M $C_6H_{12}O_6$	9.21 2.04 1.37 0.92	32
Au/C Pd/C	RHE	0.1 M NaOH + 0.1 M $C_6H_{12}O_6$	2.58 0.92	33
Indole	Ag/AgCl	1 M KOH + 0.5 M $C_6H_{12}O_6$	0.52	34
Benzothiophene	Ag/AgCl	1 M KOH + 0.5 M $C_6H_{12}O_6$	0.59	35
Ni_4Co_2/AC	Hg/HgO	3 M KOH + 1 M $C_6H_{12}O_6$	2.84	36
PdIn(90:10)/CNT	Ag/AgCl	1 M KOH + 0.5 M $C_6H_{12}O_6$	0.98	37
Pd_3Sn_2/C	Hg/HgO	0.5 M KOH + 0.5 M $C_6H_{12}O_6$	3.64	38
Au/MnO_2-C	Hg/HgO	1 M NaOH + 0.5 M $C_6H_{12}O_6$	2.50	39
PtBi/C	Ag/AgCl	0.5 M KOH + 0.05 M $C_6H_{12}O_6$	2.25	40
7% Ga@PdAgCo/CNT	Ag/AgCl	1 M KOH + 0.5 M $C_6H_{12}O_6$	2.475	This study

Empyrean) measurements were obtained for analysis of the crystal structure of the catalysts. The particle size and surface metal distribution of the catalysts were obtained by TEM (Zeiss Sigma 300). The oxidation state of the catalysts was determined by XPS (SPECS Flex) analysis. ICP-MS (Agilent 7800) was performed to determine the atomic molar ratios of the catalysts.

Electrochemical Measurements

CV, CA, and EIS analyses were applied to determine glucose electrooxidation performance of catalysts. Electrochemical measurements were carried out with a CHI 660E potentiostat device in 1 M KOH + 0.5 M $C_6H_{12}O_6$ solution. A three-electrode system consisting of a working electrode (glassy carbon), counter electrode (Pt wire), and reference electrode (Ag/AgCl) was used. CV measurements were performed at 50 mV/s in the range of −0.6 to 0.6 V. CA measurements were taken to define the stability of the catalysts at −0.4 V, −0.2 V, 0.0 V, 0.2 V, and 0.4 V. The resistance of catalysts was analyzed with EIS at −0.6–0.6 V potential range.

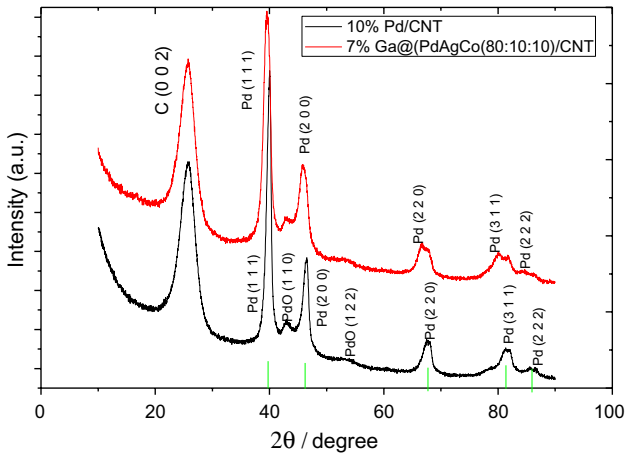

Fig. 1 XRD patterns of 10% Pd/CNT and 7% Ga@PdAgCo/CNT catalysts.

Results and Discussion

Characterization Results

XRD analysis was performed to examine the crystal structures of the catalysts. Figure 1 demonstrates XRD patterns of Pd/CNT and Ga@PdAgCo/CNT catalysts. The hexagonal structure of carbon was observed to reveal the diffraction peak of the (002) for both catalysts at approximately 25.7°. From Fig. 1, the XRD patterns of both catalysts revealed diffraction peaks at 40.1°, 46.4°, 67.7°, 81.4°, and 86.2°, corresponding to the (111), (200), (220), (311), and (222) planes of the Pd (fcc) structure (JCPDS card number 46-1043). The 2θ values at 43.0° and 53.8° corresponded to PdO (110) and PdO (122) planes for both catalysts, respectively.[41] Silver nanoparticles show planes with fcc structure. The diffraction peaks at 66.7°, 80.1°, and 84.5° correspond to (220), (311), and (222) planes of fcc structure of Ag.[42] The absence of diffraction peaks of other metals reveals that it is not observed because it is located at the same point with the Pd fcc structure or because it is in a low amount.[43] In the XRD, the negative shift pattern of the 7% Ga@PdAgCo/CNT catalyst according to 10% Pd/CNT could be due to the Ga, Ag, and Co alloys.[44] The Scherrer equation was used to calculate the crystal size of 10% Pd/CNT and 7% Ga@PdAgCo/CNT catalysts and found 9.35 and 6.48 nm, respectively.

The TEM images of catalysts are given in Figs. 2 and 3. Furthermore, particle size distribution was carried out for the catalysts. It can be seen from Figs. 2 and 3 that the generally homogeneously dispersed particles did not form agglomeration. The average particle sizes of Pd/CNT,

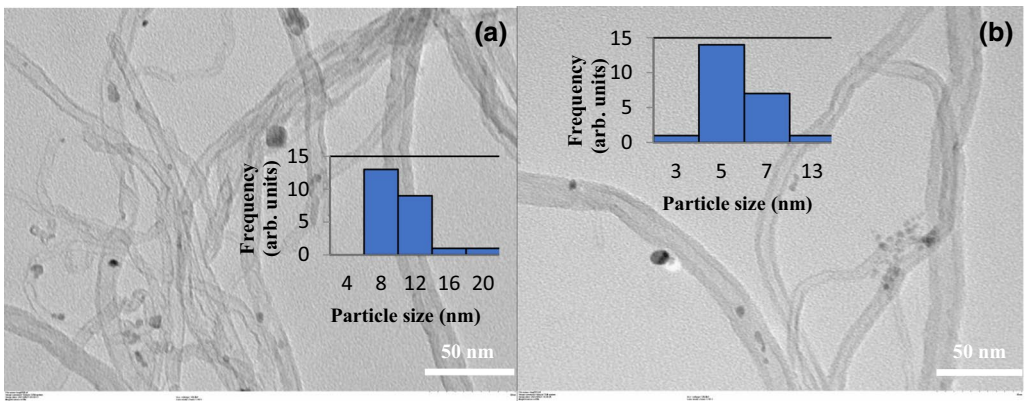

Fig. 2 TEM images of Pd/CNT (a) and PdAgCo/CNT (b) catalysts (related particle size distribution).

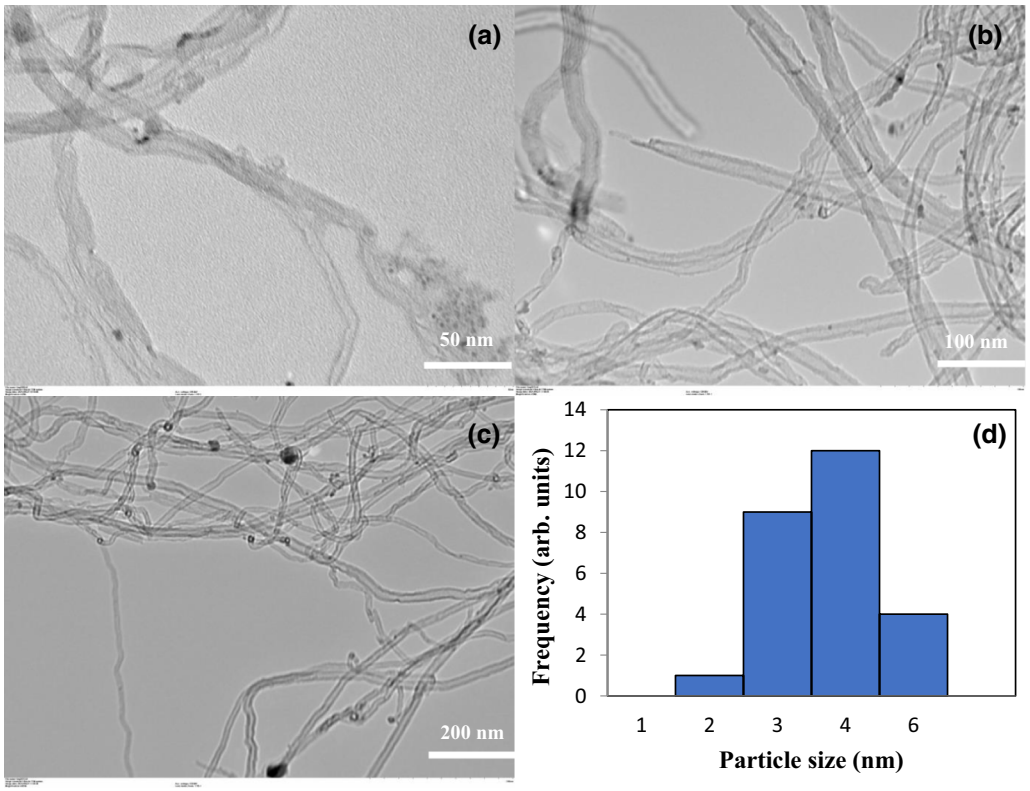

Fig. 3 TEM images of 50 nm (a), 100 nm (b), and 200 nm (c) with related particle size distribution (d) for the Ga@PdAgCo/CNT catalyst.

PdAgCo/CNT, and Ga@PdAgCo/CNT catalysts were calculated as 8.2 nm, 5.0 nm, and 3.1 nm (ImageJ program), respectively. Although the particle sizes obtained are different from the crystal size acquired in XRD, they are close to each other.[45] From ICP-MS analysis, the molar atomic ratio of Ga@PdAgCo(45:45:5:5) catalyst was found to be (12.2:78.8:0.5:8.5) by metal order. This result obtained ratios close to the desired metal ratios.

The Ga@PdAgCo/CNT catalyst was investigated by XPS analysis, which provides basic information about the chemical bonds and oxidation states of Ag, Co, Ga, and Pd. Figure 4a–f illustrates diffraction peaks of C 1s, Ag 3d, Co 2p, Ga 2p, and Pd 3d states. The binding energies of all peak positions were deconvoluted relative to C 1s of 284.6 eV. The binding energies of C 1s at 284.6 and 289.6 eV, which have two different chemical shift components, can be attributed to the C-C and O-C=O bonds, respectively.[46] The XPS spectrum of Pd 3d (Fig. 4c) clearly indicated four different peaks. The binding energies of Pd 3d (Fig. 4c) indicated four different peaks. The peaks at 335.3 eV and 340.6 eV were assigned to $3d_{5/2}$ and $3d_{3/2}$, which shows the presence of Pd^0. The other two peaks at 336.8 eV ($3d_{5/2}$) and 342.2 eV ($3d_{3/2}$) binding energies indicated that PdO was formed.[47] As seen in the XRD model (Fig. 1), the presence of PdO was also observed in the XPS analysis. Pd could be oxidized by reacting with oxygen during synthesis. Figure 4d demonstrates the presence of Ag^+ ($3d_{5/2}$ at 367.5 eV and Ag $3d_{3/2}$ at 373.5 eV) and Ag^0 ($3d_{5/2}$ at 370.4 eV and Ag $3d_{3/2}$ at 376.7 eV).[48] Fig. 4e illustrates two characteristic peaks with binding energies of 781.0 eV and 797.3 eV associated with $2p_{3/2}$ and $2p_{1/2}$, indicating the presence of Co^{2+}. Furthermore, the binding energies of Co 2p were attributed to 776.5 eV and 805.9 eV corresponding to Co3 + (2p3/2) and Co4 + (2p1/2), respectively.[49] The binding energies at 1118.0 eV and 1121.7 eV corresponded to Ga^{3+} and Ga_2O_3 of Ga $2p_{3/2}$, respectively.[50] Table II summarizes the probable chemical states of Ag 3d, C 1s, Co 2p, Ga 2p, and Pd 3d for the Ga@PdAgCo/CNT catalyst.

Electrochemical Results

The electrocatalytic activity of Pd/CNT, PdAgCo/CNT, and Ga@PdAgCo/CNT catalysts at different weight percentages was defined by CV measurements at a scan

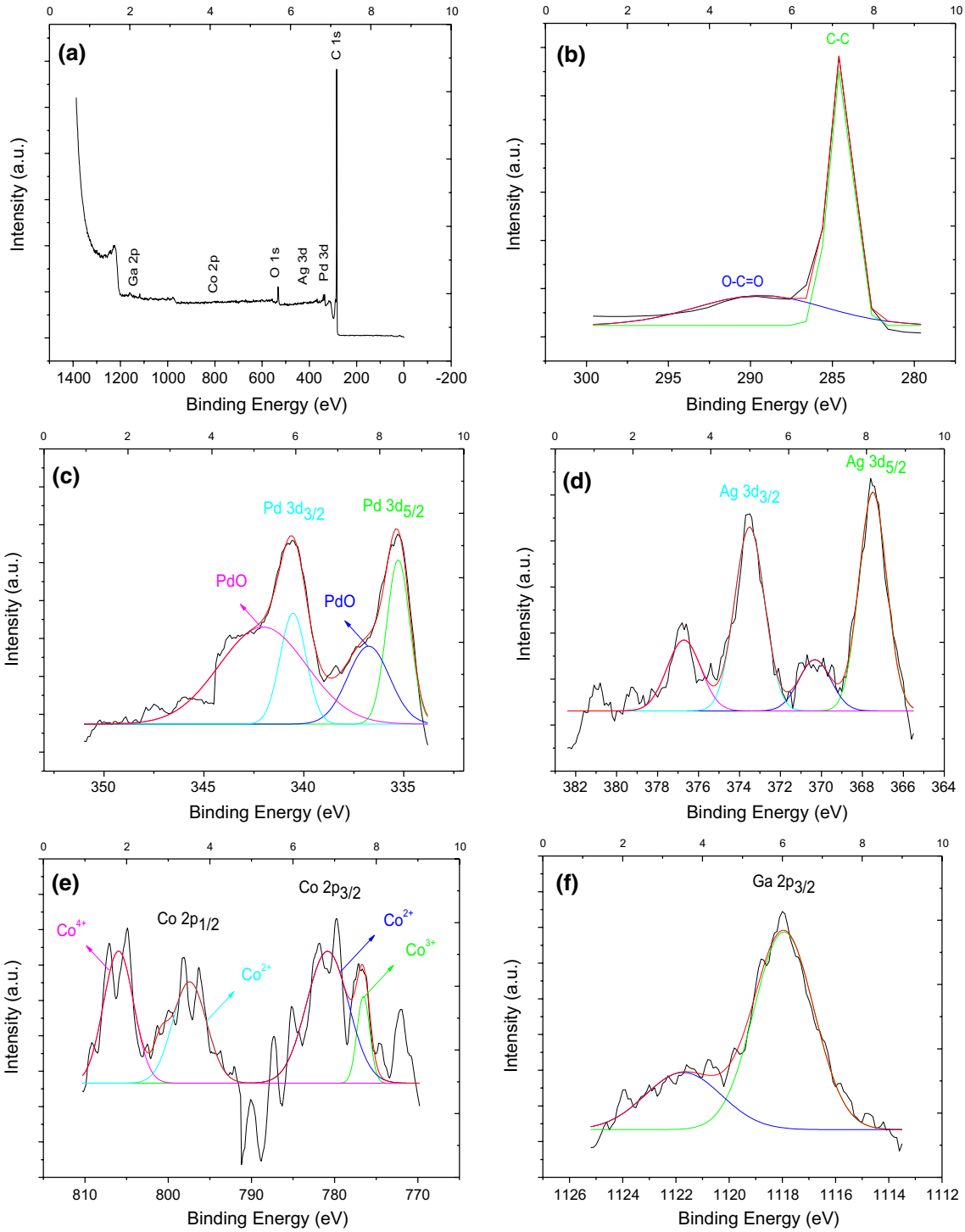

Fig. 4 XPS spectra of general spectrum (a), C 1s (b), Pd 3d (c), Ag 3d (d), Co 2p (e), and Ga 2p (f) for the Ga@PdAgCo/CNT catalyst.

rate of 50 mV/s in 1 M KOH + 0.5 M $C_6H_{12}O_6$ solution. The CV voltammograms obtained in the potential range of −0.6 to 0.6 V are presented in Fig. 5a and b. In the forward scan, glucose oxidation peaks were observed in the potential range of −0.3–0.0 V. The presence of oxidation peaks explains the electrooxidation resulting from

Table II The results of probable chemical states of Ag 3d, C 1s, Co 2p, Ga 2p and Pd 3d regions

Name	At.%	BE (eV)	Possible chemical state	Relative intensity %	Reference
C 1s	95.887	284.6	C–C	86.56	46
		289.6	O-C=O	13.44	
O 1s	3.435	532.6	–	–	
Pd $3d_{5/2}$	0.341	335.3	Pd^0	26.58	47
		336.8	PdO	23.95	
		340.6	Pd^0	24.94	
		342.2	PdO	24.53	
Ag $3d_{5/2}$	0.119	367.5	Ag^+	25.94	48
		370.4	Ag^0	24.15	
		373.5	Ag^+	25.56	
		376.7	Ag^0	24.35	
Co $2p_{3/2}$	0.095	776.5	Co^{3+}	24.90	49
		781.0	Co^{2+}	25.07	
		797.3	Co^{2+}	24.96	
		805.9	Co^{4+}	25.07	
Ga $2p_{3/2}$	0.123	1118.0	Ga^{3+}	51.10	50
		1121.7	Ga_2O_3	48.90	

glucose adsorption on the catalyst surface.[30,36] Table III contains information on the glucose electrooxidation behavior of the catalysts. The 7% Ga@PdAgCo/CNT catalyst provided the highest electrocatalytic activity as 2.475 mA/cm^2 at a peak potential of −0.161 V. The specific activity of 10% Pd/CNT and 10% PdAgCo/CNT catalysts was obtained as 0.515 mA/cm^2 and 0.867 mA/cm^2, respectively. The best glucose electrooxidation activity provided by the 7% Ga@PdAgCo/CNT catalyst is explained by the synergistic effect of Ga metal.

CA measurements were used for the electrochemical stability of the catalysts.[51] The CA measurements were taken at −0.4 V, −0.2 V, 0.0 V, 0.2 V, and 0.4 V potentials in 1000 s. Figure 6a shows the CA curves of the 7% Ga@PdAgCo/CNT catalyst at different potentials. As seen in Fig. 6a, a decrease in all potentials was observed initially due to the poisoning of the electrode surface caused by the intermediate species formed during glucose oxidation. The best catalytic activity of the 7% Ga@PdAgCo/CNT catalyst was obtained at −0.2 V potential and compared with other catalysts at −0.2 V potential in Fig. 6b. The 7% Ga@PdAgCo/CNT catalyst provided the best stability at higher current than other catalysts.

EIS analysis was used to assign the resistance of the 7% Ga@PdAgCo/CNT catalyst to glucose electrooxidation.

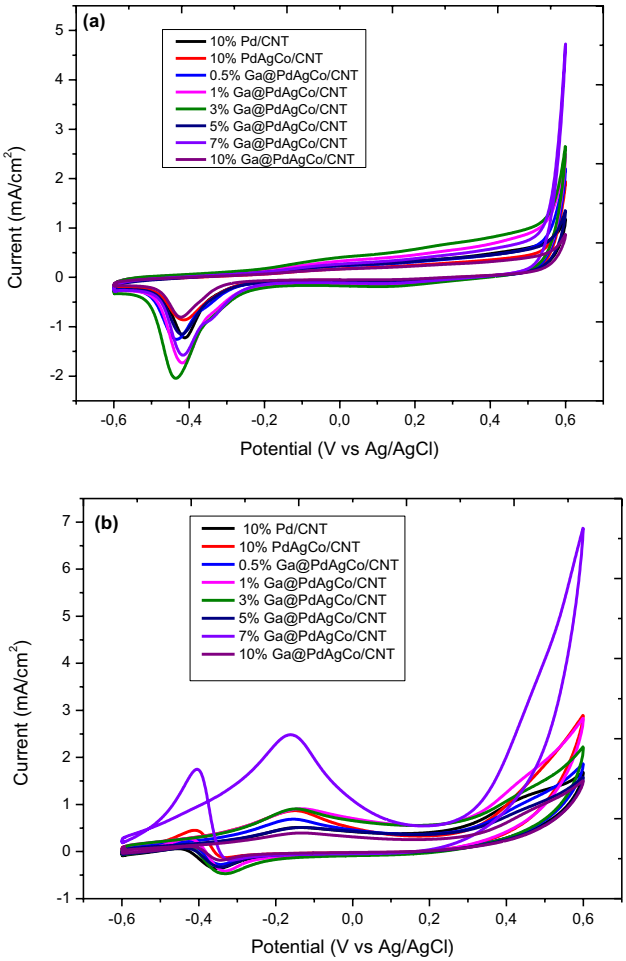

Fig. 5 Cyclic voltammograms of the catalysts (a) in 1 M KOH and (b) in 1 M KOH + 0.5 M $C_6H_{12}O_6$ solution.

For this purpose, the EIS measurements were performed in the range of −0.6–0.6 V in 1 M KOH + 0.5 M $C_6H_{12}O_6$ and Nyquist curves obtained are presented in Fig. 7a. Semicircular Nyquist curves are proportional to electrocatalytic activity. The smaller the semicircle diameter, the lower the charge transfer resistance and the higher the electrocatalytic activity.[52,53] The 7% Ga@PdAgCo/CNT catalyst exhibited the best electrocatalytic activity with lower resistance at 0.6 V potential. The Nyquist curves obtained from the measurements at 0.6 V potential of all catalysts are shown in Fig. 7b. Figure 6c demonstrates the equivalent circuit resistance model of 10% Pd/CNT, 10% PdAgCo/CNT, and 7% Ga@PdAgCo/CNT catalysts. Figure 7b reveals that the charge transfer resistance (R_{ct}) of the 7% Ga@PdAgCo/CNT catalyst is much smaller than 10% Pd/CNT (1865 Ω) and 10% PdAgCo/CNT (2572 Ω), and other catalysts showed

Table III The specific activity, mass activity, peak potential, and onset potential values of catalysts for the glucose electrooxidation

Catalyst	Specific activity, mA/cm^2	Mass activity, mA/mg Pd	Peak potential, V	Onset potential, V
10% Pd/CNT	0.515	44.47	−0.148	−0.566
10% PdAgCo/CNT	0.867	76.19	−0.150	−0.570
0.5% Ga@PdAgCo/CNT	0.689	60.85	−0.154	−0.581
1% Ga@PdAgCo/CNT	0.911	80.80	−0.137	−0.577
3% Ga@PdAgCo/CNT	0.910	82.15	−0.150	−0.583
5% Ga@PdAgCo/CNT	0.515	47.31	−0.135	−0.579
7% Ga@PdAgCo/CNT	2.475	231.08	−0.161	−0.592
10% Ga@PdAgCo/CNT	0.398	38.10	−0.135	−0.572

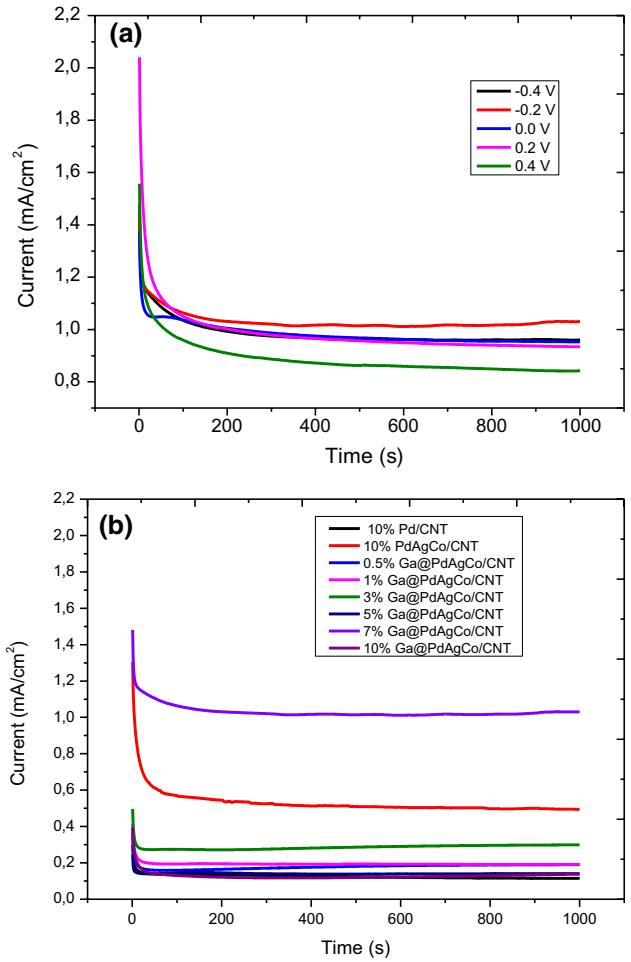

Fig. 6 Chronoamperometry curves of (a) 7% Ga@PdAgCo/CNT at different potentials and (b) comparison with other catalysts at −0.2 V in 1 M KOH + 0.5 M $C_6H_{12}O_6$.

a notable decrease in R_{ct} (632 Ω), indicating faster electron transfer and higher catalytic activity throughout glucose electrooxidation. The constant-phase elements (CPE) specified in the circuit model are R_Ω (cell ohmic resistance), R_{ct} (electrochemical kinetic-related resistance), and C_{dl} (double-layer capacitance corresponding to charge storage at the interface between the electrolyte and electrode).[54,55]

Conclusion

In the present study, the glucose oxidation activity of 10% Pd/CNT, 10% PdAgCo/CNT, and 0.5–10% Ga@PdAgCo/CNT catalysts was investigated. The 10% Pd/CNT and 10% PdAgCo/CNT catalysts were prepared by $NaBH_4$ co-reduction, and 0.5–10% Ga@PdAgCo/CNT catalysts were synthesized by $NaBH_4$ sequential reduction. The surface and structural properties of the catalysts were characterized by ICP-MS, TEM, XPS, and XRD. According to the XRD results, the crystallite size of the 7% Ga@PdAgCo/CNT catalyst calculated using the Scherrer equation was determined as 6.48 nm. TEM images confirmed that the particles were homogeneously dispersed and no agglomeration occurred. Also, the average particle size of the 7% Ga@PdAgCo/CNT catalyst calculated with the ImageJ program was very close to the value in XRD. The stability, resistance and activity of the catalysts against glucose electrooxidation were measured by CA, EIS and CV, respectively. The highest specific activity (2.475 mA/cm^2) and mass activity (231.08 mA/mg Pd) were obtained with the 7% Ga@PdAgCo/CNT catalyst. This result was explained by the synergistic effect between Ga, Pd, Co, and Ag metals that increase glucose electrooxidation. Furthermore, the addition of metals on the catalyst increased the catalytic activity because it caused an electronic state change. These results show that the 7% Ga@PdAgCo/CNT catalyst with high electrocatalytic activity is a promising anode catalyst for glucose electrooxidation.

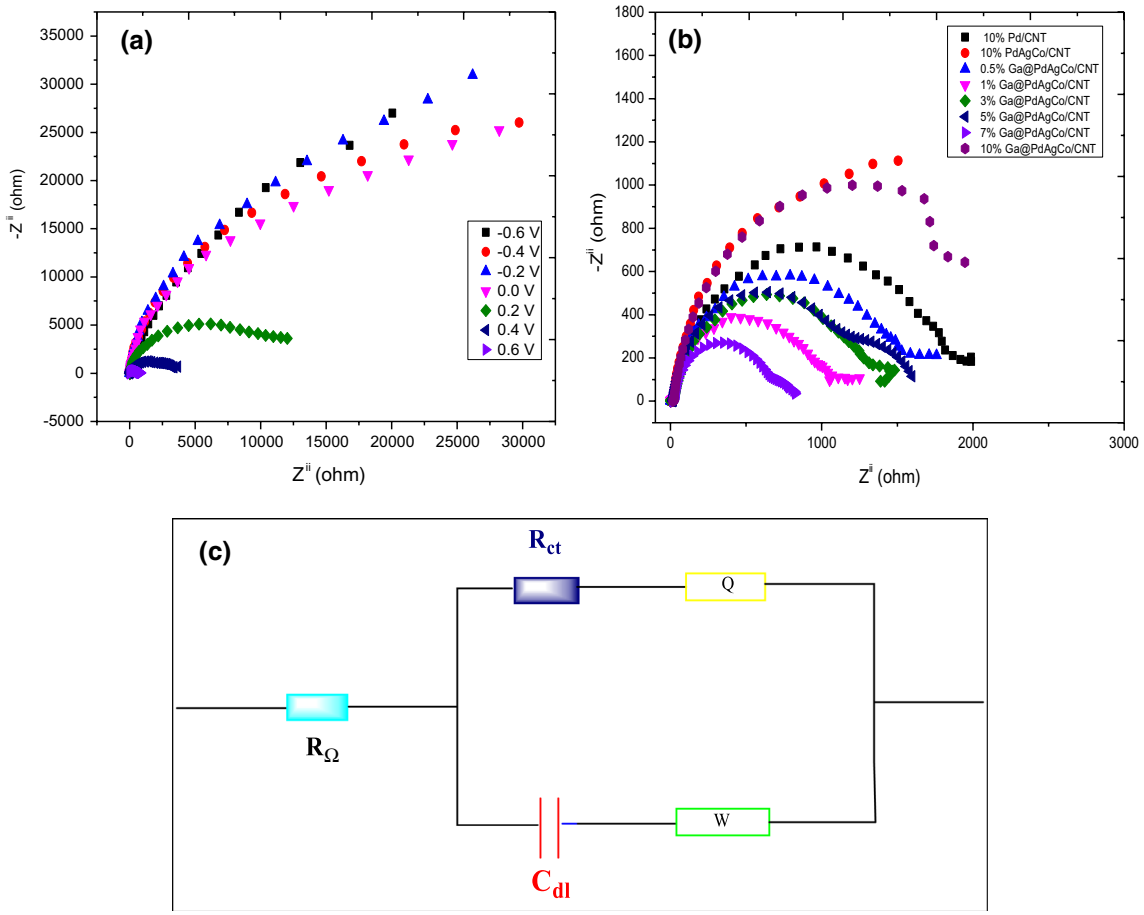

Fig. 7 Nyquist plots of (a) 7% Ga@PdAgCo/CNT at different potentials, (b) comparison with other catalysts at 0.6 V, and (c) equivalent circuit of 10% Pd/CNT, 10% PdAgCo/CNT, and 7% Ga@PdAgCo/CNT catalysts in 1 M KOH + 0.5 M $C_6H_{12}O_6$.

Conflict of interest There are no conflicts of interest to declare.

References

1. J. Zhou, X.F. Ye, L. Shao, X.P. Zhang, J.Q. Qian and S.R. Wang, *Electrochim. Acta.* 74, 267 (2012).
2. D.Y. Chung, J.M. Yoo and Y.E. Sung, *Advm Mater.* 30, 1704123 (2018).
3. Y. Wang, K.S. Chen, J. Mishler, S.C. Cho and X.C. Adroher, *Appl. Energy.* 88, 981 (2011).
4. J. Ho, Y. Li, Y.X. Dai, T. Kim, J. Wang, J. Ren, H. Yun and X.H. Liu, *Int. J. Hydrogen Energy.* 46, 20503 (2021).
5. T.C. Gentil, V.S. Pinheiro, F.M. Souza, M.L. de Araujo, D. Mandelli, B.L. Batista and M.C. dos Santos, *Renewable Energy* 165, 37 (2021).
6. M. Nacef and A.M. Affoune, *Int. J. Hydrogen Energy.* 36, 4208 (2011).
7. G.C. Liu, M. Wang, Y.T. Wang, Z. Tian and X.D. Wang, *Int. J. Energy Res.* 37, 1313 (2013).
8. A. Zadick, L. Dubau, K. Artyushkova, A. Serov, P. Atanassov and M. Chatenet, *Nano Energy* 37, 248 (2017).
9. X.Y. Shi, X.Y. Huo, O.C. Esan, L. An and T.S. Zhao, *Appl. Energy.* 297, 117145 (2021).
10. A. Eshghi and M. Kheirmand, *Int. J. Hydrogen Energy.* 42, 15064 (2017).
11. I. Tsiropoulos, B. Cok and M.K. Patel, *J. Cleaner Prod.* 43, 182 (2013).
12. X.H. Liu, M.Q. Hao, M.N. Feng, L. Zhang, Y. Zhao, X.W. Du and G.Y. Wang, *Appl. Energy.* 106, 176 (2013).
13. A. Brouzgou, L.L. Yan, S.Q. Song and P. Tsiakaras, *Appl. Catal. B.* 147, 481 (2014).
14. Y.Y. Gu, Y.C. Liu, H.H. Yang, B.Q. Li and Y.R. An, *Electrochim. Acta.* 160, 263 (2015).
15. K. Elouarzaki, A. Le Goff, M. Holzinger, J. Thery and S. Cosnier, *J. Am. Chem. Soc.* 134, 14078 (2012).
16. Y.L. Yang, X.H. Liu, M.Q. Hao and P.P. Zhang, *Int. J. Hydrogen Energy.* 40, 10979 (2015).
17. D. Basu and S. Basu, *J. Solid State Electrochem.* 17, 2927 (2013).
18. D. Basu, S. Sood and S. Basu, *Chem. Eng. J.* 228, 867 (2013).
19. A. Brouzgou and P. Tsiakaras, *Top. Catal.* 58, 1311 (2015).
20. G. Sharma, A. Kumar, S. Sharma, M. Naushad, R.P. Dwivedi, Z.A. Alothman and G.T. Mola, *J. King Saud Univ. Sci.* 31, 257 (2019).
21. H. Kivrak, D. Atbas, O. Alal, M.S. Cogenli, A. Bayrakceken, S.O. Mert and O. Sahin, *Int. J. Hydrogen Energy.* 43, 21886 (2018).
22. O. Alal, A. Caglar, H. Kivrak and O. Sahin, *Electroanalysis* 31, 1646 (2019).
23. L.H. Tian, L. Liu, Y.Y. Li, X. Feng, Q. Wei and W. Cao, *Anal. Methods.* 8, 7380 (2016).

24. C. Huang, X. Yang, H. Yang, P.Y. Huang, H.Y. Song and S.J. Liao, *Appl. Surf. Sci.* 315, 138 (2014).
25. M. Lokanathan, I.M. Patil and B. Kakade, *Int. J. Hydrogen Energy.* 43, 8983 (2018).
26. T.T. Gebremariam, F.Y. Chen, B. Kou, L.F. Guo, B.W. Pan, Q. Wang, Z. Li and W.Q. Bian, *Electrochim. Acta.* 354, 136678 (2020).
27. Y.Y. Gu, H.H. Yang, B.Q. Li and Y. An, *Electrochim. Acta.* 192, 296 (2016).
28. D. Basu and S. Basu, *Int. J. Hydrogen Energy.* 37, 4678 (2012).
29. D. Chai, X.W. Zhang, S.H. Chan and G.J. Li, *J. Taiwan Inst. Chem. Eng.* 95, 139 (2019).
30. A. Caglar, B. Ulas, O. Sahin and H. Kivrak, *Int. J. Energy Res.* 43, 8204 (2019).
31. A. Caglar, B. Ulas, O. Sahin and H.D. Kivrak, *Energy Storage.* 1, e73 (2019).
32. A. Caglar, D. Duzenli, I. Onal, I. Tersevin, O. Sahin and H. Kivrak, *Int. J. Hydrogen Energy.* 45, 490 (2020).
33. T. Rafaideen, S. Baranton and C. Coutanceau, *Appl. Catal. B-Environ.* 243, 641–656 (2019).
34. A.R. Hamad, H. Calis, A. Caglar, H. Kivrak and A. Kivrak, *Int. J. Energy Res.* 46, 1659 (2022).
35. O. Ozok, E. Kavak, O.F. Er, H. Kivrak and A. Kivrak, *Int. J. Hydrogen Energy* 45, 28706–28715 (2020).
36. M.Y. Gao, X.H. Liu, M. Irfan, J.F. Shi, X. Wang and P.P. Zhang, *Int. J. Hydrogen Energy* 43, 1805–1815 (2018).
37. O.F. Er, A. Caglar and H. Kivrak, *Mater. Chem. Phys.* 254, 123318 (2020).
38. A. Brouzgou, S. Song and P. Tsiakaras, *Appl. Catal. B.* 158, 209 (2014).
39. L. Li, K. Scott and E.H. Yu, *J. Power Sources.* 221, 1 (2013).
40. D. Basu and S. Basu, *Electrochim. Acta.* 56, 6106 (2011).
41. A. Caglar, M.S. Cogenli, A.B. Yurtcan and H. Kivrak, *Renew. Energy* 150, 78 (2020).
42. H. Pal, V. Sharma, R. Kumar and N. Thakur, *Z. Naturforsch. A: Phys. Sci.* 67, 679 (2012).
43. Q.K. Meng, S. Guo, X.Q. Zhao and S. Veintemillas-Verdaguer, *J. Alloys Compd.* 580, 187 (2013).
44. T. Ungar, *Mater. Sci. Eng. A* 309, 14 (2001).
45. B. Ulas, A. Caglar, O. Sahin and H. Kivrak, *J. Colloid Interface Sci.* 532, 47 (2018).
46. Y. Wu, Y.C. Lin and J. Xu, *Photochem. Photobiol. Sci.* 18, 1081 (2019).
47. L.J. Wang, J. Zhang, X. Zhao, L.L. Xu, Z.Y. Lyu, M. Lai and W. Chen, *Rsc Adv.* 5, 73451 (2015).
48. M.L. Ren, J.Q. Bao, P.F. Wang, C. Wang and Y.H. Ao, *Front. Chem.* 6, 489 (2018).
49. R. Zhang, Y. Lu, L. Wei, Z.G. Fang, C.H. Lu, Y.R. Ni, Z.Z. Xu, S.Y. Tao and P.W. Li, *J. Mater. Sci. - Mater. Electron.* 26, 9941 (2015).
50. C.I.M. Rodríguez, M.Á.L. Álvarez, J.D.J.F. Rivera, G.G.C. Arízaga and C.R. Michel, *ECS J. Solid State Sci. Technol.* 8, Q3180 (2019).
51. A. Caglar, T.A. Hansu, O. Sahin and H. Kivrak, *J. Electroanal. Chem.* 918, 116505 (2022).
52. M. Nacef, M.L. Chelaghmia, O. Khelifi, M. Pontie, M. Djelaibia, R. Guerfa, V. Bertagna, C. Vautrin-Ul, A. Fares and A.M. Affoune, *Int. J. Hydrogen Energy.* 46, 37670 (2021).
53. Z.X. Chen, B.B. Yu, J.J. Cao, X.L. Wen, M.H. Luo, S.Y. Xing, D. Chen, C.F. Feng, G.B. Huang and Y.X. Jin, *Electrochim. Acta.* 390, 138902 (2021).
54. J.T. Liu, Y. Xie, Y. Nan, G.L. Gou, X.Z. Li, Y.Y. Fang, X. Wang, Y. Tang, H.D. Yang and J.T. Ma, *Electrochim. Acta.* 257, 233 (2017).
55. H. Liu, M.G. George, N. Ge, D. Muirhead, P. Shrestha, J. Lee, R. Banerjee, R. Zeis, M. Messerschmidt, J. Scholta, P. Krolla and A. Bazylak, *J. Electrochem. Soc.* 165, F3271 (2018).